Table-top platform of a large scale underwater swarm

Rong Fu
Mechanics Division, Beijing Computational Science Research Center
Beijing,China
email: furong@csrc.ac.cn

Yang Ding
Mechanics Division, Beijing Computational Science Research Center
Beijing,China
Department of Physics, Beijing Normal University
Beijing,China
email: dingyang@csrc.ac.cn

Abstract—**Hydrodynamic interactions are critical in fish schooling. However, how they can be utilized in underwater swarm robots has not been sufficiently analyzed and the existing systems were not suitable to address this issue. Therefore, we have developed a table-top experimental platform by modifying miniature toy submarines (MTSs) as underwater vehicles. We used a camera, machine learning algorithms, and 2.4 GHz wireless communication module to track and individually control up to 45 MTSs in real time. The underwater swarm can achieve cohesive and stable formations similar to fish school motions, which forms the basis for the analysis of collective behavior and strategies in actual hydrodynamic environments.**

Keywords—*Underwater Swarm, Experiment Platform, Collective Motion, Submarine, Tracking-by-Detection.*

I. INTRODUCTION

Swarm robots are inspired by natural biological systems and can complete complex tasks that are far beyond the capabilities of individual robot. Underwater robot swarms have gained considerable interest for applications such as flow field analysis [1], mapping underwater environment [2, 3], ocean exploration and monitoring [4, 5], measuring ocean currents [6] and disaster prevention [7].

Animals typically move through fluids in groups because hydrodynamic interactions can reduce the energy consumption [8-11]. These interactions can also increase the stability of biological groups and may cause organisms to spontaneously form groups of specific shapes [12], as observed in bird flocks and fish schools [13, 14]. However, hydrodynamic interactions are rarely considered in underwater swarm robotic systems and how they can be utilized in these systems has not been investigated sufficiently. The existing studies have been primarily focused on multi-robot team formation and self-organized coordination [15, 16] because oceanic tasks often require the swarms to encompass large areas and the distances between the individual robots are also large. However, aggregations are sometimes necessary and beneficial during deployment and return, operations in confined environment, and so on [17].

Hydrodynamic effects have been considered in various theoretical and numerical models [12, 18, 19]. Researchers found that hydrodynamic interactions are essential for reproducing certain collective behaviors such as milling, schooling, and turning [12, 20, 21]. However, the existing hydrodynamic interaction models are all based on idealized assumptions such as inviscid or simplified empirical models to the best of the author's knowledge. The accuracy of these models and the validity strategies must be verified by conducting swarm experiments.

The behavior of collective motion is significantly affected by the scale of the system in terms of number of individuals. Some simulation studies have demonstrated that when the same control strategy is used, a drastic transition occurs when the number of individuals is increased from 10 to 20 in terms of the polarity and individual spacing group velocity [22, 23]. Therefore, the construction of large-scale systems is essential to analyze the collective behavior and control strategies of both natural and man-made systems. Large-scale underwater swarm systems (up to 120 individuals) have been previously developed for oceanic tasks; however, they are often quite bulky [24-26]. Studying these systems in a controlled hydrodynamic environment requires large pools, complex communication and positioning methods, and high endurance, which increases the cost of the overall process [26, 27].

In this study, we achieved the control of an aggregated swarm with hydrodynamic interaction using miniature toy submarines (MTSs) as underwater submersibles instead of a large and expensive platform and developed a table-top experimental platform.

II. METHOD

A. System overview

The platform setup comprises a circular pool, network camera (MV-CA020-20GC) placed vertically above the pool, multiple MTSs, wireless transmitter, and host computer, as shown in Fig. 1A. The host computer was used for the detection, tracking, and transmission of the control signals of the MTSs.

From a global perspective, computer vision technology was used for the detection and tracking of each individual MTS, and the real-time motion state information such as positions, headings, velocities, accelerations, and trajectories of the MTSs were obtained. The platform can adjust the control

algorithm based on the specific collective task, and can simultaneously control the MTS using a 2.4 GHz wireless signal. Fig. 1B depicts the workflow of the platform.
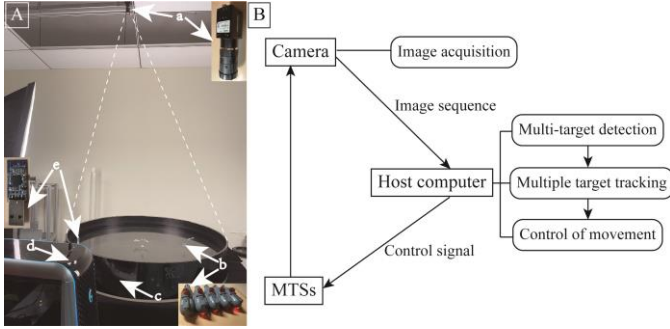
Fig. 1. (A) Overview of the platform. a. a network camera; b. underwater swarm —— miniature toy submarines; c. a circular pool, d. the host computer, e. wireless signal transmitter. (B) Design of the tracking-by-detection and control system.

B. Underwater swarm and the pool

The underwater vehicle was based on the type 016 miniature toy submarine developed by BANDAI Toy Company, shown in Fig. 2. One propeller is placed at the aft for propulsion, one propeller is placed sideways at the aft for turning, and one motor is placed at the center of the bottom to control the buoyancy by adjusting the volume of the body. TABLE I. presents the performance specifications.
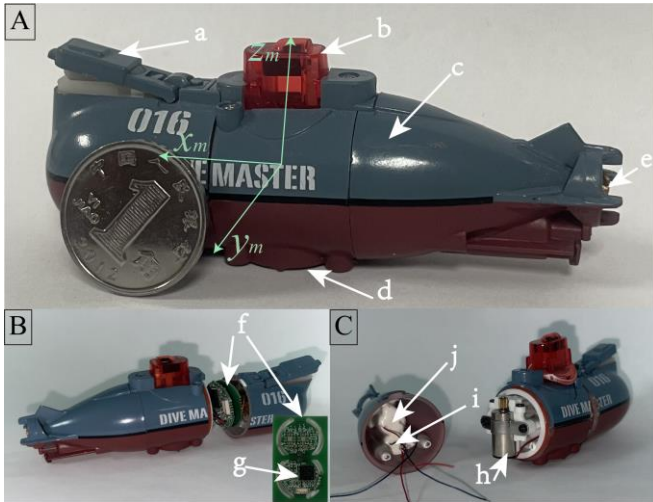
Fig. 2. Overview of miniature toy submarine design. A: Exterior. (a) power connection and charging port, (b) Infrared signal receiver (obsoleted), (c) plastic shell, (d) buoyancy system, (e) propeller. B&C: Interior (f) main control PCBs, (g) 2.4G wireless signal receiver, (h) buoyance motor, (i) steering motor, (j) main driving motor.

The original infrared control has only two channels and cannot individually control many MTSs. Therefore, it was replaced by 2.4 GHz band wireless communication module. It includes a host computer, a signal transmitter, and receivers inside the MTSs, as shown in Fig. 2g. The signal transmitter of the control module can issue approximately 1 instruction to each of 60 MTSs within one second.

The pool was a cylindrical container with a radius of 60 cm. The water area is approximately 750 times of the cross-sectional area of the submarine. This ratio ensures that the boundary effects are negligible in most positions, and is based on the information obtained in previous experiments [28-30].

TABLE I. SPECIFICATIONS OF THE MINIATURE TOY SUBMARINE

Features and Characteristics	Specifications
Size	75×20×30 mm
Weight	20 g
DOF	Surge, 150 mm/s
	Yaw, 72 °/s
Communication	Range: 1m
	Type: RF, 2.4 GHz
Energy source	Charging Duration: 25min
	Battery Life: 30min
Cost	200 Renminbi (30 USD)

C. Image capture and processing module

To track and control the MTSs, computer vision software was used. Tracking-by-detection was done based on a deep learning algorithm. The hardware and software platform of the computer was, as follows: Ubuntu18.04, NVIDIA 3070, CPU I7-10700, PyTorch, CUDA v11.1, cuDNN v8.0.2. The camera has a resolution of 1920 × 1200 @ 54 FPS and a focal length of 8 mm. The images were transmitted via Gigabit networks. The camera was placed at a point 170 cm vertically above the center of the pool.

The real-time video streams collected by the camera were converted into RGB 3-channel color image data (1920 × 1280p). The detection was performed by a modified package of *R-Centernet. Centernet* [31] is an excellent algorithm which can detect multiple targets in real time. It presents a good balance between precision and speed, and focuses on small and densely distributed targets. It reports a detected target as a point at the center of the bounding box and then estimates the key points. The *R-Centernet* [32] network model adds the rotation factor to the original *Centernet* framework. We extended the angle range returned by *R-Centernet* from 0°-180° to 0°-360° to distinguish the bow and stern of MTSs.

We trained the modified *R-Centernet* using a dataset of 2840 images of the MTSs, facilitated by *LabelImg2*. In the training process, the initial learning rate was set to 1e-5, the training epoch was set to 480, and the batch size was set to 6.

We identified each MTS after the detection by using the *Deepsort* [33] package, which is a tracking package based on Kalman filtering and frame-by-frame data association. Angle information was added as a new channel to the four existing channels, i.e., central point abscissa, central point ordinate, bounding box width, and bounding box height.

D. MTS control methods

The steering angular speeds of the MTSs cannot be controlled proportionally, and can only be tuned by switching the steering motor on or off, which is known as Bang–Bang control [34]. We first consider the control in a continuous manner and then convert the control output to Bang–Bang control output.

Path following of a single MTS.

To test the controllability, we first controlled a single MTS to follow a trajectory by implementing a proportional-differential (PD) control algorithm [35]. The target point moved along the trajectory and the MTS moved towards the target point. The current state of the MTS was described by the position, X, and the orientation, θ. The orientation error, e_R, and distance error, e_D, between the MTS and the target were calculated based on the current position of the target trajectory, $X_T(x_T(t), y_T(t))$, shown in Fig. 3A. We defined:

$$\begin{cases} \hat{X}(t) = X(t) + Vdt \\ e_D(t) = |X_T(t) - X(t)| \\ e_R(t) = \theta - \theta_{e_D} \end{cases} \qquad (1)$$

where $\hat{X}(t)$ denotes the prediction of the position at the next frame based on the current position and velocity of MTS, V represents the current velocity of MTS (~0.75 BL/s), dt is set to 50 ms, based on the time interval of two successive frames.
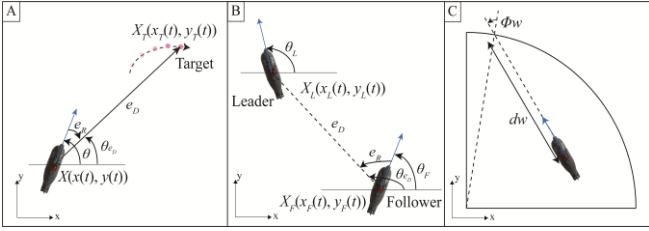
Fig. 3. Input parameters of the control of an MTS. (A) The current pose of an MTS (x, y, θ), the target point (x_T, y_T), the orientation error, e_R, and distance error, e_D, in a trajectory following case. The target travels along a timed sequence of points on a trajectory, which are represented by the pink dots. (B) The relative position and angle of a follower (x_F, y_F) to the leader (x_L, y_L) in the follower-leader case. (C) The distance, d_W, separates the position of the MTS from its current point of impact on the wall; Φ_W denotes the angle between the heading of the MTS and the angular position of current point of impact with respect to the center of the tank.

We used two independent PD controllers to achieve position and direction control. This strategy can be applied to the case of low coupling between the forward propulsion and steering force. The controller is expressed as:

$$\begin{aligned} a_f &= K_{p1} \cdot e_D(t_k) + K_{d1} \cdot \frac{e_D(t_k) - e_D(t_{k-1})}{\Delta t}, \quad K_{P1} > 0, K_{d1} > 0 \\ a_r &= K_{p2} \cdot e_R(t_k) + K_{d2} \cdot \frac{e_R(t_k) - e_R(t_{k-1})}{\Delta t}, \quad K_{P2} > 0, K_{d2} > 0 \end{aligned} \qquad (2)$$

where, a_f and a_r control the actions of the main drive motor and steering motor, respectively, $K_{p1} = 1$, and $K_{p2} = 1$ are the proportional gains, and $K_{d1} = 1$ and $K_{d2} = 0.05$ are the derivative gains. Because we ultimately implemented Bang–Bang control, proportional gains were set as unity for convenience. $\Delta t = 0.05s$ represents the time interval between two successive frames.

The main motor generates forward thrust along the x_m-axis direction of the MTS (see Fig. 2) and the steering motor generates torque about the z_m-axis to control the left or right turn of the MTS. Based on the PD controller, the calculated control values are converted to motor action signals using a control signal converter which is expressed as follows:

$$\begin{aligned} forward\ signal &= \begin{cases} forward & if\ |a_f| > F_{th} \\ stop & otherwise \end{cases} \\[6pt] steering\ signal &= \begin{cases} turn\ left & if\ a_r > R_{th} \\ turn\ right & if\ a_r < -R_{th} \\ stop & otherwise \end{cases} \end{aligned} \qquad (3)$$

where $F_{th} = 6$ and $R_{th} = 2$ represent the control signal thresholds along the forward and rotation directions, respectively. The thresholds are used to ensure that the output control signal is turned off when it is within a small range.

The MTSs move much faster (2 BL/s) than conventional underwater vehicles [36] and are therefore difficult to control, since a transmitter can transmit only approximately 60 action signals (motion / stop) to an MTS in 1 second. Therefore, we reduced the swim speed and angular velocity of the MTS by adjusting the duty ratio between the motion signal and the stop signal within a certain period of time (~200 ms and 4 frames). For forward control, the duty cycle was set at 25%, indicating that the computer transmitted 1 forward signal for every 4 frames and transmitted 1 stop signal for the remaining 75% of the time. For steering control, the duty cycle was set at 50%, indicating that 2 out of every 4 frames emits the steering signal (left or right turn) and stops steering for the remaining 50% of the time.

Collective motion of multiple MTSs. To control the swarm, we implemented the leader–follower strategy as an example and test case. Based on the fish school model [37], the leader was designed to avoid collision with the arena boundary. We set the target turning speed, $\omega^*(t)$, as follows:

$$\omega^*(t) = \text{sgn}(\phi_W)/d_W \qquad (4)$$

where, d_W (cm) and ϕ_W (degree) represent the distance and angle between the MTS and the point on the wall respectively; further details are presented in Fig. 3C. The turning speed $\omega^*(t)$ values are converted to motor steering action signals as follows:

$$steering\ signal = \begin{cases} turn\ left & if\ \omega^* > R_{th} \\ turn\ right & if\ \omega^* < -R_{th} \\ stop & otherwise \end{cases} \qquad (5)$$

where, $R_{th} = 0.03$ determines the repulsion strength from the wall on the leader.

The following MTSs attempt to follow the leader without collision and maintain angular alignment with the leader when the distance is sufficiently short. The orientation error of the follower MTS corresponding to the desired direction is described by $e_R(t)$, and the position error of the follower MTS corresponding to the leader MTS is described by $e_D(t)$. When $e_D(t)$ is greater than 3BL (body length), the desired direction is set to point towards the leader. When the distance is small, the desired direction is set to match the orientation of the leader (see Fig. 3B). We defined:

$$e_D(t) = \left| X_L(t) - X_F(t) \right|$$

$$e_R(t) = \begin{cases} \theta_F - \theta_{e_D} & if \ e_D(t) > 3BL \\ \theta_F - \theta_L & otherwise \end{cases} \quad (6)$$

where, $X_L(t)$ and $X_F(t)$ denote the positions of the leader and follower, respectively, $\theta_L(t)$ and $\theta_F(t)$ indicate the orientations of the leader and follower, respectively, and θ_{e_D} represents the direction of the vector from the center of the follower to the center of the leader. We used the PD controller described in (2) for position and direction control. The calculated control values were converted to motor action signals using (3), while considering the values of $F_{th} = 16$ and $R_{th} = 20$.

In this task, as the number of MTSs increased, the existing communication bandwidth was no longer sufficient to adjust the duty ratio. Consequently, more time was required for the master controller of the centralized control method to receive and process all the information from the MTSs [27]. Therefore, we fixed the swimming speeds, which means forward signal is always on, and only controlled the heading directions of the MTSs.

Each MTS was controlled by a separate thread in the computer even though the control signals were transmitted by the same hardware. The ID given by the detection and tracking program must be matched with the ID for wireless communication to achieve individual control over the MTSs. This problem was solved by sequentially transmitting a forward signal at the beginning of reach run to each individual MTS while maintaining a gap of 500 ms, to look for the MTS with the highest velocity during each period of time. Subsequently, a table was created for the pairs of the IDs and MTSs in the images.

III. RESULTS

A. Hydrodynamic interaction in the near-field

Our test results demonstrated the hydrodynamic interaction when an advancing MTS passed by the side of a stationary MTS. The main effect was manifested in the change of angular velocity, which did not significantly affect the velocity. Fig. 4A, B depicts the positional states of the two MTSs at t=2 s and t=9 s. When MTS2 swims past the side, the heading angle of

MTS1 turns by approximately 20 degrees in 7 s. The results demonstrate that a strong hydrodynamic interaction is observed when the minimal distance is approximately 0.5 BL.
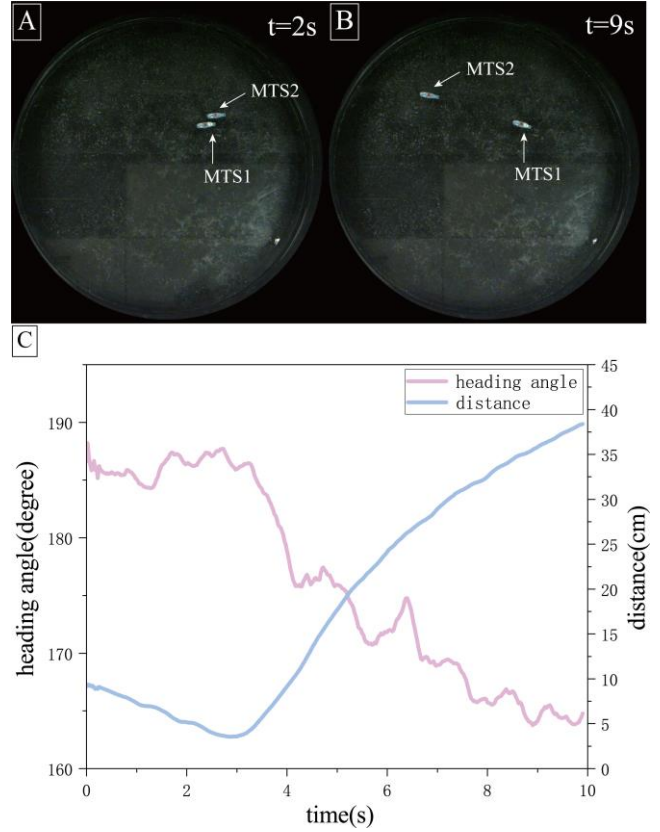
Fig. 4. Hydrodynamic interaction of an MTS swimming past a stationary MTS. (A)&(B) The postures of the two MTSs at t=2 s and t=9 s. (C) The pink curve indicates the orientation angle of MTS1 with time, and the blue curve indicates the distance between two MTSs as a function of time.

B. Target detection and tracking

Accurate and robust information on the current MTSs' postures is required to drive them in water. Up to 45 MTSs can be detected and tracked accurately by the proposed system. The average frame rate of real-time target detection is 22 FPS, which drops to 21 FPS when tracking is included (see Fig. 5).

C. Path following of a single MTS

We tested the tracking and control ability of the system by commanding a single MTS to follow a hexagon or a lemniscate curve. For both curves, four replicate experiments were performed, and the average deviation from the predefined path is 0.465 BL. The experimental results (in Fig. 6A, B) demonstrate that a good control performance was achieved when different forms of curves were considered as the desired paths.

D. Collective motion of multiple MTSs

Stable schooling behaviors of the MTSs were obtained from a random initial condition, which show that the platform can effectively control the collective MTSs (see Fig. 6C, D). The current control method can be used to form a swarm of up to 12 MTSs. The existing leader-follower strategy achieves less

cohesive motion for more MTSs and effective strategies with consideration of hydrodynamic interactions for larger swarms require further research.
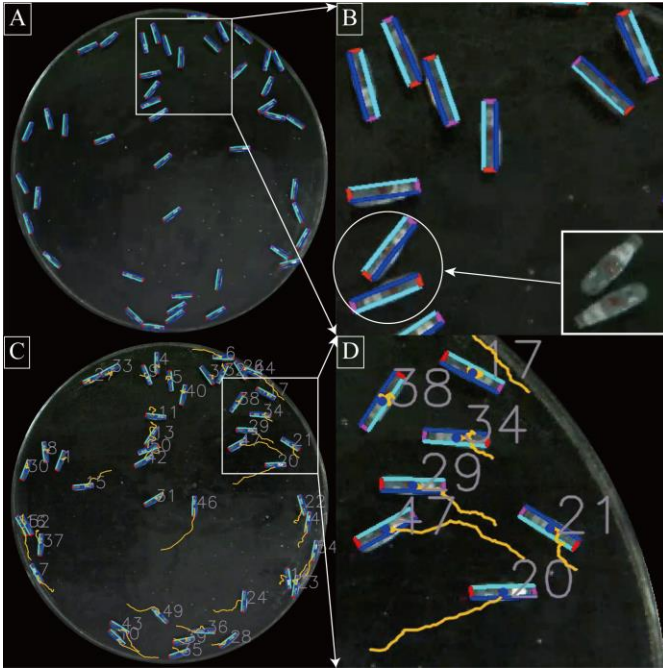
Fig. 5. Results of tracking-by-detection. (A) A sample image of multi-target detection. (B) Close-up view of subfigure A, the red lines indicate the bows of the MTSs and the pink lines indicate the sterns of the MTSs. Inset shows the original image. (C) Sample images of multi-target tracking. (D) Close-up view of subfigure C; the yellow curves represent the trajectories of the MTSs and the gray numbers near the MTS represent ID numbers in the tracking program.
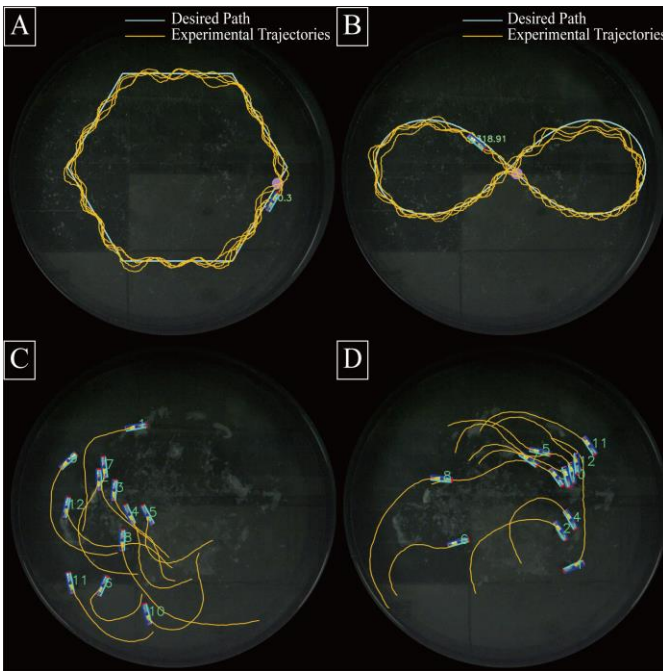
Fig. 6. Controlled motion of MTSs. Path following of a hexagon curve (A) and figure-of-eight curve by a single MTS. The blue curve represents the prescribed path, the yellow curves represent the actual path traced by the MTS, and the pink points represent the current targets of the MTSs. (C)&(D)

Snapshot of the MTSs and their trajectories (yellow lines) from the leader-follower experiments.

E. Time delay in the system

Certain delays occur when controlling the swarm because various processes must be performed, from the movement of the MTS at a certain instant to the observation of its state and then to the movement control. A delay of up to 25 ms can occur during the process of capturing images owing to the capture frame rate of the network camera (approximately 40 FPS). Following the image capture, the latency increases during the detection and tracking of dozens of MTSs using the computer vision technology in the host computer. The video frame rate is reduced from 40 FPS to approximately 22 FPS during the Target-Detection of the original video stream, after which the Target-Tracking of the video stream is performed, and the frame rate is reduced to approximately 21 FPS.

For a single MTS, the motion of the propeller of the MTS to the position at which the command is based on faces a delay between 50 ms to 350 ms. The lower limit is obtained by measuring the time between the completion of the image acquisition and the signal transmission in the software. The upper limit is estimated by measuring the time between the acquisition of an image and the acquisition of an image that shows a noticeable motion of the MTS.

IV. CONCLUSIONS

In this study, an experimental platform of an underwater robot swarm was developed. The platform can perform real-time tracking and detection to realize control strategies based on positions, orientations, and velocities. It can be used to analyze the effect of hydrodynamic interactions in underwater swarms because the propulsion mechanism and overall shape are similar to real underwater vehicles. Including these effects in control algorithms may be crucial for certain tasks of underwater swarms and can help obtain a better understanding of the behavior of fish schools. In the future, we aim to increase the pool size and the throughput of the control signals by adding more transmitters, which can decrease time delays and improve the control accuracy.

REFERENCES

[1] A. Hackbarth, E. Kreuzer and E. Solowjow, "HippoCampus: A micro underwater vehicle for swarm applications," in 2015 IEEE/RSJ International Conference on Intelligent Robots and Systems (IROS), 2015, pp. 2258-2263: IEEE.

[2] P. C. Abreu and A. M. J. I.-P. Pascoal, "Formation control in the scope of the MORPH project. Part I: Theoretical foundations," vol. 48, pp. 244-249, 2015.

[3] P. C. Abreu, M. Bayat, A. M. Pascoal, J. Botelho, P. Góis, J. Ribeiro et al., "Formation Control in the scope of the MORPH project. Part II: Implementation and Results," vol. 48, pp. 250-255, 2015.

[4] A. L. Christensen, M. Duarte, O. Postolache, S. Sargento, M. Oliveira, P. Santana et al., "Design of communication and control for swarms of aquatic surface drones," 2015.

[5] M. Duarte, V. Costa, J. Gomes, T. Rodrigues, F. Silva, S. M. Oliveira et al., "Evolution of collective behaviors for a real swarm of aquatic surface robots," vol. 11, p. e0151834, 2016.

[6] J. S. Jaffe, P. J. Franks, P. L. Roberts, D. Mirza, C. Schurgers, R. Kastner et al., "A swarm of autonomous miniature underwater robot

drifters for exploring submesoscale ocean dynamics," vol. 8, pp. 1-8, 2017.

[7] C. Wong, E. Yang, X.-T. Yan and D. Gu, "An overview of robotics and autonomous systems for harsh environments," in 2017 23rd International Conference on Automation and Computing (ICAC), 2017, pp. 1-6: IEEE.

[8] S. Marras, S. S. Killen, J. Lindström, D. J. McKenzie, J. F. Steffensen, P. J. B. e. Domenici et al., "Fish swimming in schools save energy regardless of their spatial position," vol. 69, pp. 219-226, 2015.

[9] P. A. Dewey, D. B. Quinn, B. M. Boschitsch and A. J. J. P. o. F. Smits, "Propulsive performance of unsteady tandem hydrofoils in a side-by-side configuration," vol. 26, p. 041903, 2014.

[10] D. J. N. Weihs, "Hydromechanics of fish schooling," vol. 241, pp. 290-291, 1973.

[11] E. J. A. S. Shaw, "Schooling fishes: the school, a truly egalitarian form of organization in which all members of the group are alike in influence, offers substantial benefits to its participants," vol. 66, pp. 166-175, 1978.

[12] A. Filella, F. Nadal, C. Sire, E. Kanso and C. J. P. r. l. Eloy, "Model of collective fish behavior with hydrodynamic interactions," vol. 120, p. 198101, 2018.

[13] T. Vicsek and A. J. P. r. Zafeiris, "Collective motion," vol. 517, pp. 71-140, 2012.

[14] S. Li, C. Li, L. Xu, W. Yang and X. J. A. S. Chen, "Numerical simulation and analysis of fish-like robots swarm," vol. 9, p. 1652, 2019.

[15] T. Zhang, Y. Li, S. Li, Q. Ye, C. Wang, and G. J. a. p. a. Xie, "Decentralized Circle Formation Control for Fish-like Robots in the Real-world via Reinforcement Learning," 2021.

[16] F. Berlinger, M. Gauci and R. J. S. R. Nagpal, "Implicit coordination for 3D underwater collective behaviors in a fish-inspired robot swarm," vol. 6, 2021.

[17] N. Shlyakhov, I. Vatamaniuk and A. Ronzhin, "Survey of methods and algorithms of robot swarm aggregation," in Journal of Physics: Conference Series, 2017, vol. 803, no. 1, p. 012146: IOP Publishing.

[18] Z.-M. Yuan, C.-Y. Ji, A. Incecik, W. Zhao and A. J. O. E. Day, "Theoretical and numerical estimation of ship-to-ship hydrodynamic interaction effects," vol. 121, pp. 239-253, 2016.

[19] J. A. Carrillo, Y.-P. Choi and S. P. Perez, "A review on attractive–repulsive hydrodynamics for consensus in collective behavior," in Active Particles, Volume 1: Springer, 2017, pp. 259-298.

[20] D. S. Calovi, U. Lopez, S. Ngo, C. Sire, H. Chaté, and G. J. N. j. o. P. Theraulaz, "Swarming, schooling, milling: phase diagram of a data-driven fish school model," vol. 16, p. 015026, 2014.

[21] U. Lopez, J. Gautrais, I. D. Couzin and G. J. I. f. Theraulaz, "From behavioural analyses to models of collective motion in fish schools," vol. 2, pp. 693-707, 2012.

[22] H. Kunz and C. K. J. A. l. Hemelrijk, "Artificial fish schools: collective effects of school size, body size, and body form," vol. 9, pp. 237-253, 2003.

[23] S. V. Viscido, J. K. Parrish and D. J. E. m. Grünbaum, "The effect of population size and number of influential neighbors on the emergent properties of fish schools," vol. 183, pp. 347-363, 2005.

[24] T. Schmickl, R. Thenius, C. Moslinger, J. Timmis, A. Tyrrell, M. Read et al., "CoCoRo--The self-aware underwater swarm," in 2011 Fifth IEEE Conference on Self-Adaptive and Self-Organizing Systems Workshops, 2011, pp. 120-126: IEEE.

[25] D. Sutantyo, P. Levi, C. Möslinger and M. Read, "Collective-adaptive lévy flight for underwater multi-robot exploration," in 2013 IEEE International Conference on Mechatronics and Automation, 2013, pp. 456-462: IEEE.

[26] B. Arbanas, T. Petrovic and S. Bogdan, "Consensus protocol for underwater multi-robot system using scheduled acoustic communication," in 2018 OCEANS-MTS/IEEE Kobe Techno-Oceans (OTO), 2018, pp. 1-5: IEEE.

[27] J. Connor, B. Champion and M. A. J. I. S. J. Joordens, "Current algorithms, communication methods and designs for underwater swarm robotics: A review," vol. 21, pp. 153-169, 2020.

[28] K. Suzuki, T. Takagi and T. J. F. R. Hiraishi, "Video analysis of fish schooling behavior in finite space using a mathematical model," vol. 60, pp. 3-10, 2003.

[29] N. Tarcai, C. Virágh, D. Ábel, M. Nagy, P. L. Várkonyi, G. Vásárhelyi et al., "Patterns, transitions and the role of leaders in the collective dynamics of a simple robotic flock," vol. 2011, p. P04010, 2011.

[30] L. Lei, R. Escobedo, C. Sire and G. J. P. c. b. Theraulaz, "Computational and robotic modeling reveal parsimonious combinations of interactions between individuals in schooling fish," vol. 16, p. e1007194, 2020.

[31] X. Zhou, D. Wang and P. J. a. p. a. Krähenbühl, "Objects as points," 2019.

[32] M. Wang, J. Wang and C. Liu, "Remote sensing image rotation object detection based on key points (in Chinese)." vol. 35, pp. 102-108, 2021.

[33] N. Wojke, A. Bewley and D. Paulus, "Simple online and realtime tracking with a deep association metric," in 2017 IEEE international conference on image processing (ICIP), 2017, pp. 3645-3649: IEEE.

[34] M. R. Caputo and M. R. Caputo, Foundations of dynamic economic analysis: optimal control theory and applications. Cambridge University Press, 2005.

[35] G. F. Franklin, J. D. Powell and M. L. Workman, Digital control of dynamic systems. Addison-wesley Reading, MA, 1998.

[36] T. Wang, X. Peng, G. Pan and D. J. A. S. E. T. Xu, "Decelopment and Key Technologies of Unmanned U nderwater Vehicles," vol. 1, pp. 52-64, 2017.

[37] J. Gautrais, F. Ginelli, R. Fournier, S. Blanco, M. Soria, H. Chaté et al., "Deciphering interactions in moving animal groups," 2012.